UNIVERSITY OF BIRMINGHAM
University of Birmingham Research at Birmingham

Fabrication of gradient hydrogels using a thermophoretic approach in microfluidics

Kosmidis Papadimitriou, Alexandros; Chong, Shin Wei; Shen, Yi; Lee, Oisin Stefan; Knowles, Tuomas P J; Grover, Liam M; Vigolo, Daniele

DOI:
10.1088/1758-5090/ad2b05

License:
Creative Commons: Attribution (CC BY)

Document Version
Publisher's PDF, also known as Version of record

Citation for published version (Harvard):
Kosmidis Papadimitriou, A, Chong, SW, Shen, Y, Lee, OS, Knowles, TPJ, Grover, LM & Vigolo, D 2024, 'Fabrication of gradient hydrogels using a thermophoretic approach in microfluidics', *Biofabrication*, vol. 16, no. 2, 025023. https://doi.org/10.1088/1758-5090/ad2b05

Link to publication on Research at Birmingham portal

General rights
Unless a licence is specified above, all rights (including copyright and moral rights) in this document are retained by the authors and/or the copyright holders. The express permission of the copyright holder must be obtained for any use of this material other than for purposes permitted by law.

•Users may freely distribute the URL that is used to identify this publication.
•Users may download and/or print one copy of the publication from the University of Birmingham research portal for the purpose of private study or non-commercial research.
•User may use extracts from the document in line with the concept of 'fair dealing' under the Copyright, Designs and Patents Act 1988 (?)
•Users may not further distribute the material nor use it for the purposes of commercial gain.

Where a licence is displayed above, please note the terms and conditions of the licence govern your use of this document.

When citing, please reference the published version.

Take down policy
While the University of Birmingham exercises care and attention in making items available there are rare occasions when an item has been uploaded in error or has been deemed to be commercially or otherwise sensitive.

If you believe that this is the case for this document, please contact UBIRA@lists.bham.ac.uk providing details and we will remove access to the work immediately and investigate.

Download date: 01. May. 2024

Biofabrication

CrossMark

OPEN ACCESS

RECEIVED
17 October 2023

REVISED
28 January 2024

ACCEPTED FOR PUBLICATION
20 February 2024

PUBLISHED
4 March 2024

Original content from this work may be used under the terms of the Creative Commons Attribution 4.0 licence.

Any further distribution of this work must maintain attribution to the author(s) and the title of the work, journal citation and DOI.

PAPER

Fabrication of gradient hydrogels using a thermophoretic approach in microfluidics

Alexandros Kosmidis Papadimitriou[1], **Shin Wei Chong**[2,5], **Yi Shen**[3,4,5], **Oisin Stefan Lee**[2], **Tuomas P J Knowles**[3], **Liam M Grover**[1] and **Daniele Vigolo**[1,2,5,*]

[1] School of Chemical Engineering, University of Birmingham, Edgbaston, Birmingham B15 2TT, United Kingdom
[2] The University of Sydney, School of Biomedical Engineering, Sydney, NSW 2006, Australia
[3] Department of Chemistry, University of Cambridge, Lensfield Road, Cambridge CB2 1EW, United Kingdom
[4] The University of Sydney, School of Chemical and Biomolecular Engineering, Sydney, NSW 2006, Australia
[5] The University of Sydney Nano Institute, University of Sydney, Sydney, NSW 2006, Australia
[*] Author to whom any correspondence should be addressed.

E-mail: daniele.vigolo@sydney.edu.au

Keywords: thermophoresis, microfluidics, hydrogels, stiffness gradients, osteoblasts

Supplementary material for this article is available online

Abstract

The extracellular matrix presents spatially varying physical cues that can influence cell behavior in many processes. Physical gradients within hydrogels that mimic the heterogenous mechanical microenvironment are useful to study the impact of these cues on cellular responses. Therefore, simple and reliable techniques to create such gradient hydrogels are highly desirable. This work demonstrates the fabrication of stiffness gradient Gellan gum (GG) hydrogels by applying a temperature gradient across a microchannel containing hydrogel precursor solution. Thermophoretic migration of components within the precursor solution generates a concentration gradient that mirrors the temperature gradient profile, which translates into mechanical gradients upon crosslinking. Using this technique, GG hydrogels with stiffness gradients ranging from 20 to 90 kPa over 600 μm are created, covering the elastic moduli typical of moderately hard to hard tissues. MC3T3 osteoblast cells are then cultured on these gradient substrates, which exhibit preferential migration and enhanced osteogenic potential toward the stiffest region on the gradient. Overall, the thermophoretic approach provides a non-toxic and effective method to create hydrogels with defined mechanical gradients at the micron scale suitable for *in vitro* biological studies and potentially tissue engineering applications.

1. Introduction

Cell behavior involved in biological processes from embryogenesis to disease progression is regulated by an intricate interplay between cells and a complex milieu of biochemical and biophysical signals within their microenvironment [1–3]. Although chemical signals, such as cytokines and extracellular matrix (ECM)-bound growth factors, have been long appreciated as key players in directing normal physiology and pathological processes, there is an increasing recognition that matrix mechanics can have a significant impact on these processes as well [4]. Of all, matrix stiffness has been widely recognized as a major regulator of cell adhesion [5], migration [6], proliferation [7], and stem cell fate [8, 9]. Beyond basic variation in the range of mechanical stiffness across different tissue types, heterogeneities in the spatial matrix organization also result in variation on the local tissue level, typically in the form of gradients. For instance, tissue stiffening following injury creates a stiffness gradient away from the wound site which promotes fibroblast cell recruitment to aid wound healing [10], whereas increased ECM stiffness during breast tumorigenesis has been linked to increased propensity of aggressive cancer cell invasion [11]. Stiffness gradients can also occur through natural variation within tissues, for example, in the tissue interfacing tendons and bones known as enthesis [12, 13].

© 2024 The Author(s). Published by IOP Publishing Ltd

In order to investigate how such variations in spatial matrix stiffness contribute to direct local cell activity in health and diseased states, a number of methods have been developed to create stiffness gradient substrates *in vitro*. These are, for example, controlled UV photopolymerization using gradient or sliding photomasks [14, 15], microfluidic gradient generators [16], embedding rigid substrates in a soft substrate [6], and assembly of microgels generated with varying composition of precursor solution [17]. However, most of the existing methods are technically complex, show poor reproducibility, or are limited in the stiffness range and gradient strength that can be produced [18, 19]. The gradient and sliding photomask techniques are among the most popular approaches due to its simplicity, but they are generally limited to shallow gradients and present potential cytotoxicity issues from photoinitiators that remained within the polymerized substrate [9, 20].

Crucially, the choice of hydrogel used for cell culture systems in cell biology studies and tissue engineering is primarily dependent on the specific question or application [21]. Despite diverse methods for fabricating continuous gradient substrates however, they are often specific to a particular crosslinking mechanism, limiting their widescale applicability to cater for the growing number of new hydrogel systems being developed in recent years [15, 22, 23]. Thus, we aim to develop a non-toxic, versatile route of fabricating gradient substrates that works independently of the hydrogel polymerization scheme, whilst still providing users fine control of the gradient properties down to micron-scale resolution suitable to probe cell-substrate interactions. To demonstrate this, we fabricated 600 μm-wide gradient hydrogel strips and showed that these substrates presented continuous gradients of physical properties which in turn endowed them with spatially distinct osteogenic capacity.

2. Results and discussion

2.1. Fabrication of stiffness gradient hydrogel

Recently, a new microfluidic technique to fabricate stiffness gradient hydrogels by exploiting the physical phenomenon of thermophoresis was described [24]. Using this technique, local manipulation of the properties of a hydrogel was achieved by carefully imposing and controlling temperature gradients across a microfluidic channel containing the hydrogel precursor solution (figure 1(a), top). To visualize the thermophoretic process, we filled the microfluidic channel with 500 nm green fluorescent beads (prepared as 1% aqueous solution). Then, one side of the channel was heated while the other side of the channel was cooled, using the same system design that would later be employed for fabricating gradient hydrogels as described below. Figure 1(a) (bottom) demonstrates that the fluorescent beads readily accumulate toward the cold side of the microchannel within 45 min, in the direction of the thermophoretic force. This result confirmed that thermophoresis can indeed be used to induce particle motion within micron-scale confinements [25], which behavior we expect to be similar for biopolymer molecules.

Toward recapitulating the biophysical characteristics of enthesis (~500 μm width) [26], here we use the proposed technique to demonstrate the fabrication of Gellan gum (GG) gradient hydrogels spanning a physiologically relevant stiffness range across a 600 μm-wide strip. GG is a naturally derived polysaccharide which forms a strong gel via sol-gel transition upon cooling in the presence of divalent cations such as calcium ions [27, 28]. Due to its high biocompatibility and tuneability, GG substrates have demonstrated its versatility as scaffolds for tissue engineering applications, especially for cartilage or osteochondral tissues [29–31].

By carefully imposing and controlling temperature gradients across a microfluidic channel filled with an initially homogenous aqueous GG solution, we exploited thermophoresis to form a concentration gradient of GG polymer coils inside the microchannel, which directly translates into stiffness and porosity gradients upon GG polymerization.

Thermophoresis is a transport phenomenon in which solutes dispersed in a solution migrate towards the hot side or the cold side along a temperature gradient [25, 32]. This migration is dependent upon the specific solute-solvent interactions [33], the solute size [34, 35], the average temperature [36], and the type of electrolytes dispersed in solution [37]. The presence of a temperature gradient generates a mass flux, J_m, which can be characterized by the Brownian mass diffusion coefficient, D, and the thermophoretic mobility, D_T, following:

$$J_m = -\rho\left[D\frac{\mathrm{d}c}{\mathrm{d}x} + c(1-c)D_T\frac{\mathrm{d}T}{\mathrm{d}x}\right]$$

where ρ is the density of solute, c is the concentration, and T is the temperature. The direction of the induced concentration gradient would be along the same axis as the imposed temperature gradient, defined here as the x-direction. Once steady state is reached and there is no net movement of solutes ($J_m = 0$), the resulting concentration gradient is balanced by the temperature gradient:

$$\frac{\mathrm{d}c}{\mathrm{d}x} = -c(1-c)S_T\frac{\mathrm{d}T}{\mathrm{d}x}$$

where $S_T = D_T/D$ is the so called Soret coefficient. S_T is defined as positive when solutes accumulate toward

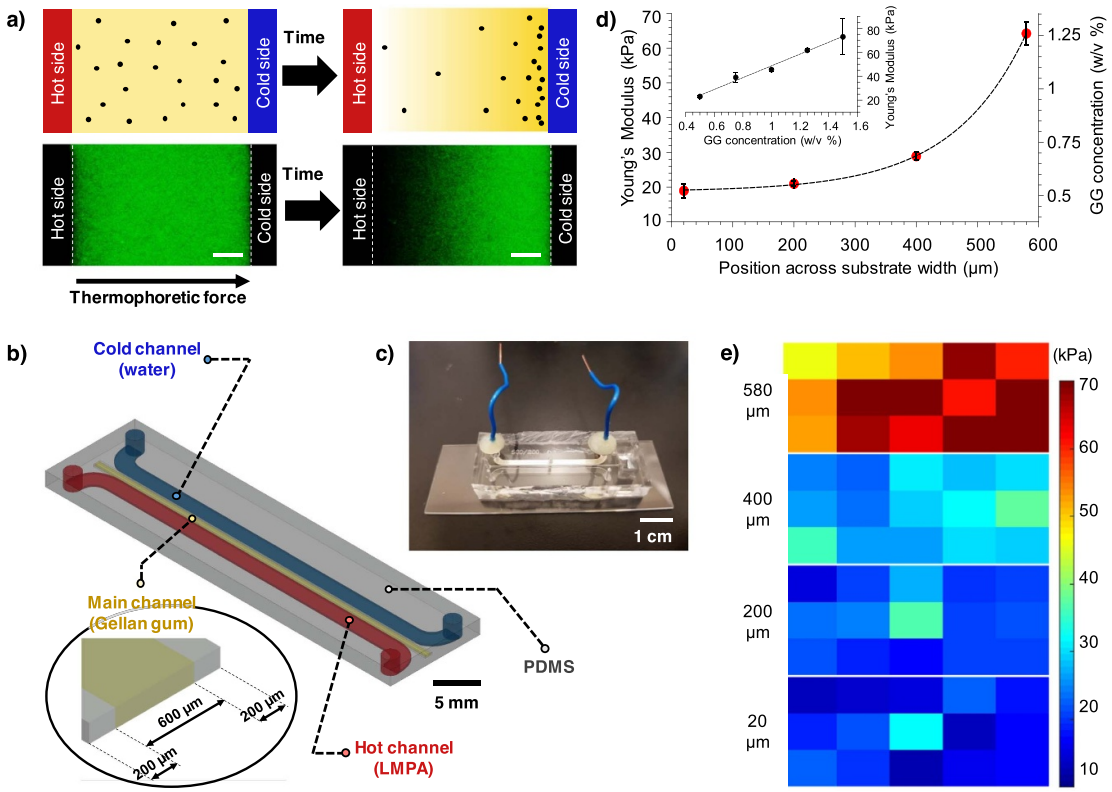

Figure 1. Fabrication of GG stiffness gradient hydrogel in microfluidics. (a) Thermophoresis results in directed migration of solutes along the temperature gradient (top). This phenomenon is experimentally visualized using 500 nm fluorescent polystyrene nanoparticles suspension (1% in water) inside a microfluidic channel (bottom), scale bar: 100 μm. (b) Schematic illustration of the microfluidic device which consists of a main sample channel and two side channels used to generate a temperature gradient across the main channel. (c) Image of the assembled microfluidic device. (d) Young's modulus (left axis) and the corresponding local GG concentration (right axis) across the width of a gradient substrate prepared using 1% w/v initial Gellan gum concentration, 7.5 °C mm^{-1} temperature gradient, and 30 min application time. The dashed line is an exponential fit. Inset shows the dependence of GG hydrogel stiffness on the concentration used, obtained by measuring a range of known concentration uniform samples. Error bars represent standard error. (e) Corresponding analyzed force maps taken at four different points across the width of the substrate; at each point, samples were indented in a 15-point grid with a 20 μm × 20 μm surface area.

the cold side and negative otherwise. Crucially, thermophoresis takes place following the characteristic mass diffusion time as a function of diffusion distance and solute characteristic size via the Stokes–Einstein equation. Given the micron-scale dimensions of microfluidic channels and hydrogel macromer sizes on the order of nanometers, thermophoresis thus presents a convenient method to create microscale gradient substrates (demonstrated within 1 h in this study).

We used a microfluidic chip with a main sample channel and two side channels to impose a temperature gradient across the main channel containing aqueous GG solution in the presence of calcium ions, as described in the materials and methods section (figures 1(b) and (c)). The solution was maintained in its uncrosslinked state by keeping the whole microfluidic system above the sol-gel transition temperature of GG (approximately 40 °C for 0.5–1.5 w/v% GG with 5 mM calcium ions [38]), enabling gradual redistribution of the GG polymer chains via thermophoretic migration. Once the desired concentration gradient was achieved within the microfluidic device, rapid crosslinking was induced by promptly decreasing the temperature below the critical gelation temperature [39], in order to preserve the gradient profile and translate the concentration gradient into a stiffness gradient. We then extruded the material by gently applying pressure manually with a syringe filled with deionized water at the inlet of the microchannel. In this way we obtained a 600 μm wide, 4 cm long and 140 μm height substrate which exhibited a stiffness gradient across its width (figures 1(d) and (e)). Initially, we also performed stiffness measurements at different lengths along the gradient gel, confirming that the generated stiffness gradient profile is consistent throughout the entire substrate.

Compared to our previous study based on ionic crosslinking alginate hydrogels [24], this microfluidic system was modified to work with thermosensitive hydrogels by simply attaching the device onto a thermoelectric Peltier module which provides rapid regulation of the system average temperature,

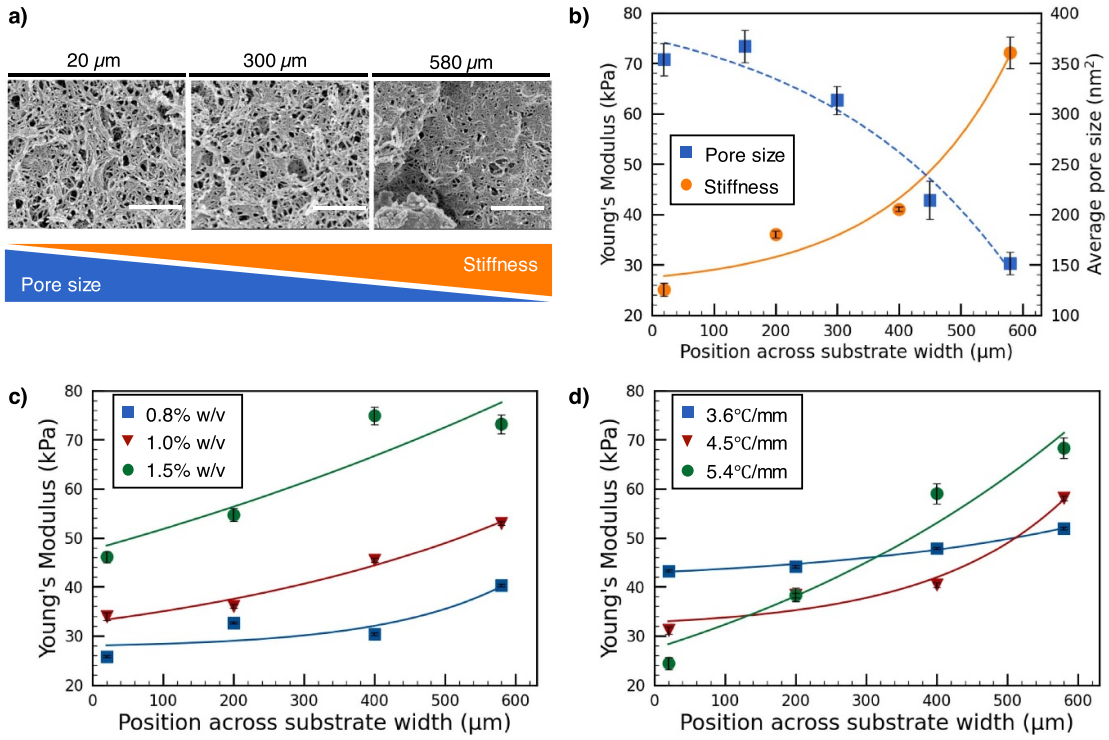

Figure 2. Characterization of gradient GG hydrogels. (a) Representative SEM images taken at multiple locations across the substrate width, scale bars: 500 nm. (b) The pore size of fabricated GG hydrogels decreased proportionally with increasing stiffness along the gradient. (c) Young's modulus for hydrogels prepared with 0.8% w/v, 1.0% w/v, and 1.5% w/v GG concentration at a fixed temperature gradient of 4.5 °C mm^{-1}. (d) Young's modulus for hydrogels prepared with 3.6 °C mm^{-1}, 4.5 °C mm^{-1}, and 5.4 °C mm^{-1} applied temperature gradient with a fixed initial GG concentration of 1% w/v. All lines are an exponential fit, error bars represent standard error.

and thus, user-controlled onset of GG gelation. Ultimately, this fabrication concept can also be applied to various types of hydrogels and crosslinking scheme. For example, the same microfluidic system described here can be used for photopolymerizable hydrogels such as gelatin methacryloyl and poly (ethylene glycol) diacrylate. In this case, the whole microfluidic device can be exposed to UV light to enable gradient hydrogel formation following thermophoretic manipulation of local compositions across the precursor solution. We can expect the resulting stiffness gradient to similarly mirror the shape of applied temperature gradient, but the achievable gradient strength would likely vary due to differing physicochemical properties of the polymer chains.

2.2. Mechanical and structural characterization

We determined the local Young's modulus across the width of fabricated GG gradient hydrogels by performing force-indentation measurements in liquid using atomic force microscopy (AFM), see the materials and methods section for details. For hydrogels prepared with 1% w/v initial GG concentration and 7.5 °C mm^{-1} applied temperature gradient, we observed a stiffness gradient spanning 20–80 kPa over a distance of 600 μm (figure 2(b)). We also characterized uniform stiffness GG hydrogels prepared using different GG concentrations and verified that the substrate stiffness increases linearly with concentration (inset in figure 1(c)). Then, the concentration-stiffness data can be used as a calibration master curve to estimate the concentration profile across the fabricated stiffness gradient GG hydrogels based on their Young's modulus measurements. These results support the idea that the application of thermophoresis in microfluidics can effectively generate a solute concentration gradient within an initially homogenized solution, and convective effects inside the microchannel are insignificant [25]. Furthermore, by maintaining the orientation of the hydrogel after extrusion, we were able to confirm that the stiffest region was along the edge of sample nearest to the cold channel. This indicates that the Soret coefficient of the GG solution is positive and GG coils experience a driving force toward the lower temperature region of the device [24].

Because higher degrees of crosslinking are known to result in smaller pore sizes, we also expected an accompanying porosity gradient associated with the formation of concentration gradient [40, 41]. Indeed, scanning electron microscopy (SEM) images taken at multiple locations on the surface of the 1% w/v GG hydrogels (7.5 °C mm^{-1} applied temperature) revealed an average pore size transitioning from the

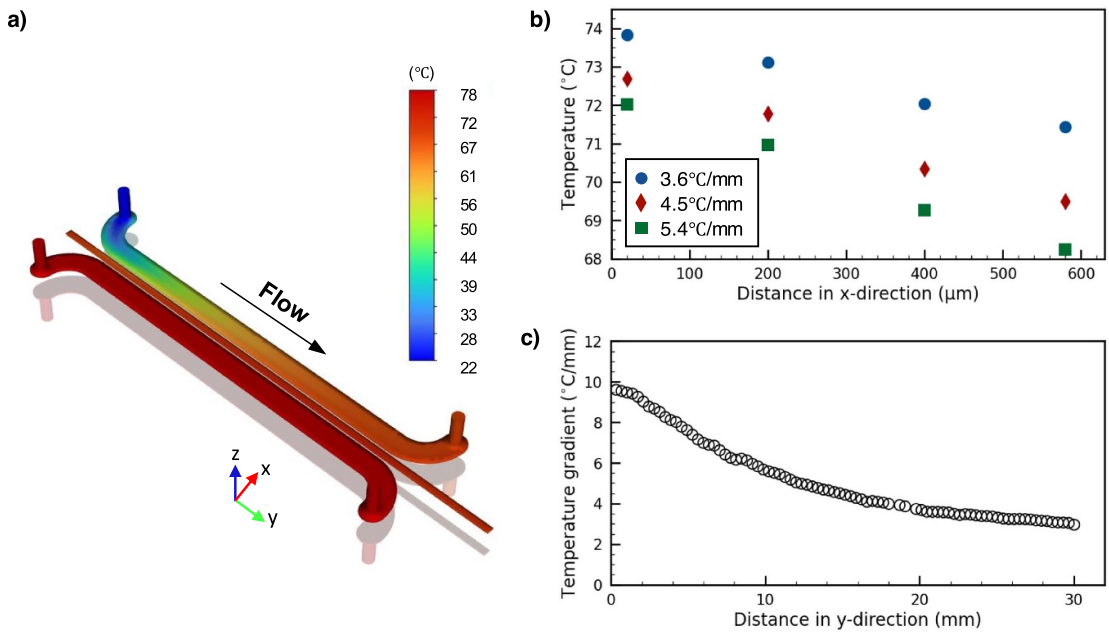

Figure 3. Computational simulation of temperature profile. (a) Example simulation of temperature profile across the microfluidic system, based on experimental conditions for 4.5 °C mm^{-1} applied temperature gradient. (b) Temperature distribution across the channel width for 3.6 °C mm^{-1}, 4.5 °C mm^{-1}, and 5.4 °C mm^{-1}, measured at the middle section of the device. (c) Variation in the strength of temperature gradient along the channel length, simulated for experimental water flowrate of 300 μl min^{-1}.

largest (∼350 nm^2) at the soft ends to the smallest (∼150 nm^2) at the stiff ends (figures 2(a) and S1).

We further demonstrated the capability of this technique to create stiffness gradients of varying range and gradient strengths. An increase in the concentration of initial GG concentration resulted in a higher hydrogel stiffness overall (figure 2(c)), while steeper gradients were achieved by increasing the temperature difference across the microfluidic system (figure 2(d)). In principle, the concentration gradient generated using this thermophoretic mechanism exhibits an exponential profile, which is also reflected in the resulting stiffness gradient [33]. This exponential profile becomes more pronounced with increasing temperature gradient strength. Conversely, this means that linear stiffness gradient hydrogels could practically still be fabricated with milder applied temperature gradients (e.g. <3.5 °C mm^{-1}) by maintaining a smaller temperature difference between the hot and cold side channels. Because the resulting concentration gradient only adopts a subtle exponential profile, the concentration (and thus stiffness) would appear to vary linearly over the entire width of the substrate, thereby yielding linear stiffness gradient gels. The stiffness gradients measured here have a range spanning several native tissues, such as muscle (∼20 kPa) and pre-mineralized bone (>30 kPa) [42]. While this represents a moderately stiff regime within the physiological mechanical landscape, which could be explained by the inherently stiffer nature of GG hydrogels, a lower or higher range of stiffnesses could be achieved by using an alternative hydrogel choice [42].

2.3. Evaluation of temperature profile across the microfluidic system

In this method, characterization of the temperature profile across the microfluidic system is essential to allow correlation with the corresponding concentration gradient, and thus, stiffness gradient in the final hydrogel substrate. Experimentally, we estimate the actual temperature gradient across the main channel from an electrical resistance analogue model, as described previously [24] and complemented here in the supplementary material. Using the system described here, it is important to note that the temperature will always assume a linear variation across the main sample channel. To verify this [24], we evaluated the temperature distribution across the whole system by performing computational simulations over the virtual microfluidic model (figure 3(a)). We confirmed that the temperature across the main microfluidic channel decreases linearly from the hot side to the cold side, and the strength of temperature gradient (figure 3(b)) is directly proportional to that of the stiffness gradients (figure 2(d)) yielded experimentally. Furthermore, we examined the effects of varying water flowrates in the 'cold' channel on the uniformity of temperature gradients produced along the axis of channel length (figures 3(c) and S3). In all cases, the temperature of the Joule heater was assumed to be constant. Simulation of the experimental flowrate of 300 μl min^{-1} revealed that the temperature gradient is highest near the inlet, which gradually decays toward a plateau along the length of the device (figure 3(c)). This could be attributed to the progressive heating of water as it flows

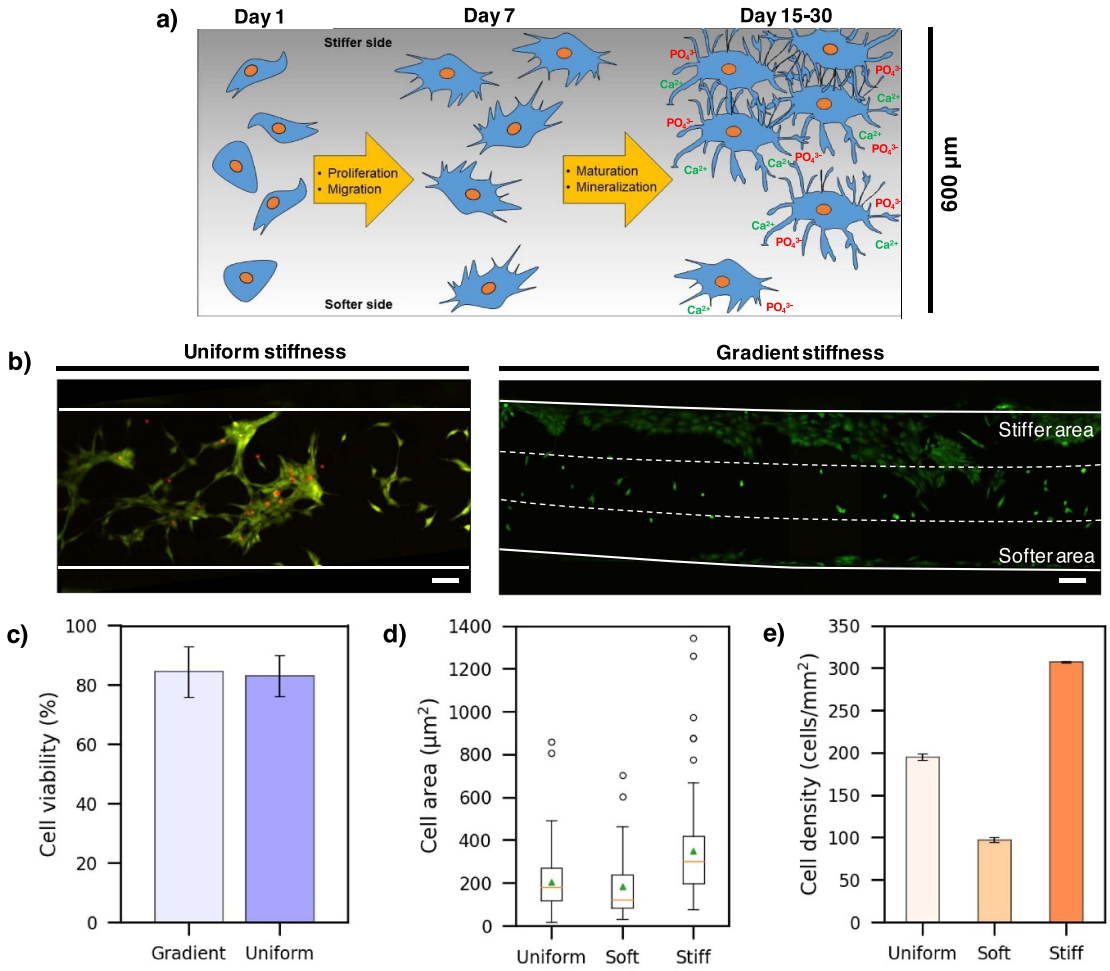

Figure 4. MC3T3 cell behavior on stiffness gradient GG hydrogel. (a) Schematic representation of MC3T3 osteoblast cell activity in response to stiffness gradient. (b) Representative confocal images showing the live (green) and dead (red) cells distribution after 7 d of culture on GG substrates with uniform stiffness (left; control sample) and stiffness gradient (right). (c) Cell viability, (d) cell spreading and (e) cell density after 7 d of culture on gradient substrates. Scale bars: 100 μm. Error bars in (c) and (e) represent standard error. For the box and whisker plots in (d), individual green triangles represent the average value for the indicated condition, and the orange lines represent the median value.

through the channel, but because only a small (1–2 cm) section of the fabricated GG hydrogels were utilized in subsequent cell culture studies, we were able to obtain reasonably uniform stiffness gradient substrates as verified by AFM measurements. While we acknowledge that gradient hydrogel platforms that are amenable to higher production levels would be required to render them useful for cell culture applications, in this proof-of-concept study, we focused on demonstrating the applicability of the thermophoretic technique to fabricate GG gradient hydrogels for cell-based studies. Importantly, the results clearly show that the stiffness gradient profile can be controlled simply by tuning the temperature distribution within the microfluidic system. For future development, it would be possible to leverage the inherent change in temperature gradient along the microchannel to fabricate multiple hydrogels with different stiffness gradient strengths concurrently within the same device.

2.4. Stiffer regions promoted cell migration and osteogenic mineralization

It has been extensively reported in literature that stem cell lineage specification and maturation of progenitor cells can be directed *in vitro* using engineered matrix mimicking the elasticity of the native tissue of interest [8, 43, 44]. We therefore postulated that osteogenic cells cultured on GG gradient hydrogels spanning the osteoid tissue ranges (>30 kPa) will show enhanced osteogenic activity toward the stiffer region of the substrate in a mechanical dose-dependent manner (figure 4(a)), as a first demonstration of the utility of this platform for interrogating stiffness-dependent behavior.

We first measured cell viability through the relative volumes of calcein-AM and propidium iodide positive cells, indicating live and dead cells, respectively. Observation after 7 d showed a high cell viability of ∼85% on uncoated GG hydrogels (figure 4(c)), confirming the nontoxic fabrication process as well

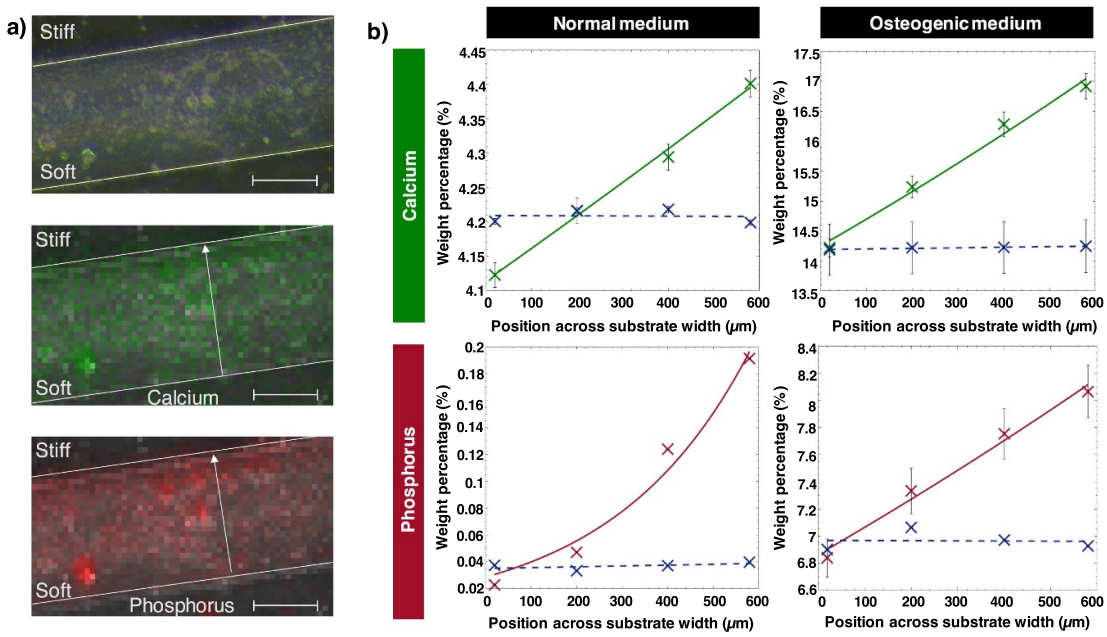

Figure 5. Mineral deposition after 30 d of culture. (a) Representative brightfield (top) as well as calcium (middle) and phosphorus (bottom) x-ray fluorescence images for cells grown on stiffness gradient GG hydrogels, scale bars: 300 μm. (b) Calcium and phosphorus content measured on substrates with gradient (continuous lines) or uniform (dashed lines) stiffness. Across all substrates, mineral deposition was further promoted when cells were cultured in osteogenic medium compared to normal medium. Error bars represent standard error.

as the biocompatibility of pure GG hydrogels for cell culture. We also performed 2D confocal imaging at Days 1, 3, and 7 to investigate cell spreading and migration in response to a stiffness gradient (figures 4(b) and S4). We calculated cell spreading as the cell area and further evaluated cell migration by calculating the distribution of cell densities across the substrate surface over 7 d. The results showed more spreading (figure 4(d)) and migration (figure 4(e)) toward stiffer regions of the substrate. Furthermore, the cell area and cell density were found to be lower on the softer region of the gradient substrate (20–30 kPa) compared to the control sample (∼50 kPa). Presumably, the hydrogel density affected these cellular responses since stiffer matrices generally cause cells to spread more due to higher formation of focal adhesion complexes [45, 46], and cells can exhibit directional migration along stiffness gradients through a biological process known as durotaxis [19, 47, 48]. In this study, variation in mechanical stiffness is directly related to the hydrogel concentration level and consequently the degree of cross-linking. While cell behavior is influenced by the substrate mechanical stiffness, it is also important to consider potential confounding effects due to variation in pore architecture. However, in the context of probing stiffness-dependent cellular behavior on planar substrates, matrix porosity was found to have no interacting effects on these behaviors [41].

We further examined the effects of stiffness in modulating the extent of substrate mineralization, which is an indicator of MC3T3 cells differentiation into mature osteoblast phenotype [48]. To investigate the degree of mineralization, we performed x-ray fluorescence (XRF) to quantify the amount of calcium and phosphorus (phosphate) deposition on the GG substrates after culturing for 15 or 30 d (figures 5(a) and S5(a)). The distribution of calcium and phosphorus content consistently showed a gradient pattern which increases from the soft to stiff side of the GG hydrogel, meaning stiffer substrates promoted maturation of preosteoblast cells (figures 5(b) and S5(b)). It is interesting to note that despite the stiffness of the control sample being within the range of the stiffer region of the gradient substrate (40–70 kPa), overall, the cells exhibited lower amount of mineral deposition on the uniform gels compared to the gradient gels. One possible explanation to this is due to the stiffness-induced migration and increased proliferation rate of cells along the stiffness gradient. Additionally, to probe the interplay between chemical and mechanical factors, we compared the mineralization activity of cells cultured in normal and osteogenic media. The latter resulted in an upregulated calcium and phosphorus deposition on both uniform and gradient stiffness GG hydrogels, and the mineral deposits were similarly distributed in a stiffness-dependent fashion. Altogether, our results add to the wealth of existing literature which suggest that matrix mechanics play an equally, if not more significant role in controlling osteoblast cell function and behavior [49, 50]. Crucially, this also highlights that a method capable of locally manipulating the matrix mechanics at the micron-scale offers tremendous opportunities

to create scaffolds with pre-programmed cues toward engineering complex physiological tissues *in vitro*. In this study, we limit our scope to only generating linear gradients, but more complex gradient shapes can be achieved depending on the design of microfluidic network for heating and cooling.

3. Conclusions

Hydrogels have become a ubiquitous tool to organize and present a range of biophysical cues that mimic the native ECM. In recent years, this has proven to be particularly useful as a reductionist model system to probe cell-ECM interactions and better understand how isolated mechanical cues drive cell behavior. In view of the ubiquity of stiffness gradients within biological tissues, a new technique to fabricate stiffness gradient hydrogels via controlled redistribution of unreacted precursor components by exploiting thermophoretic effects in microfluidics was proposed recently [24]. In this study, we demonstrated the application of this technique to fabricate 600 μm-wide GG hydrogel strips with tunable stiffness range and gradient strength. Using these hydrogels spanning a physiologically relevant elastic moduli range of ∼20–100 kPa, we observed that osteoblast precursor cells cultured on the substrates exhibited directed migration and increased mineralization tendency toward stiffer regions on the gradient. Moreover, the mineralization activity was further enhanced when cells were cultured in supplemented osteogenic medium compared to regular medium, highlighting the synergistic effects of biochemical and biophysical factors in orchestrating cell behavior and function. In comparison to the most commonly used gradient photomask method and other strategies based on controlling the light exposure during hydrogel crosslinking [14, 15, 51], the proposed thermophoretic approach can be applied to various types of hydrogels irrespective of their crosslinking mechanism, thus is not restricted to solely photo-crosslinkable biomaterials. Here we demonstrated the generation of stiffness gradients which are relatively steep, but shallower gradients and/or overall softer substrates can also be obtained by tuning the applied temperature gradient and initial hydrogel concentration, respectively. This feature would enable the fabrication of stiffness gradients covering the full mechanical landscape of physiological (∼1 Pa μm^{-1}) and pathological (>10 Pa μm^{-1}) conditions [19], which has been a difficult technical challenge to tackle using most existing stiffness gradient systems. Another important feature of this thermophoretic technique is that the microfluidic channel configuration can be customized to create more complex gradient patterns, whilst maintaining a smooth gradient profile down to micron-scale resolution. Altogether, we envision that this generic and versatile technique may significantly advance the relevance of gradient hydrogel systems for *in vitro* biological studies, and have far-reaching impacts on the broad fields of biomaterials and mechanobiology. For instance, the thermophoretic technique could be a valuable tool for programming hydrogels with spatially defined micro-scale cues that can robustly guide short-term cell activity toward engineering tissues *in vitro* for disease modelling and tissue engineering applications.

4. Materials and methods

4.1. Materials

Gelzan™ CM, poly (ethyleneimine) solution analytical standard 50% (w/v) in H_2O, minimum essential medium eagle (alpha modification, with sodium bicarbonate, without L-glutamine, ribonucleosides and deoxyribonucleosides, liquid, sterile-filtered, suitable for cell culture), fetal bovine serum (US origin sterile-filtered), phosphate buffer saline (liquid, sterile-filtered, DPBS Modified 10*X*, without calcium, without magnesium, suitable for cell culture), L-glutamine, β-glycerophosphate disodium salt hydrate (BioUltra, suitable for cell culture, suitable for plant cell culture, ⩾99%) and trypsin-EDTA solution (1*x*, sterile-filtered, BioReagent, suitable for cell culture, 0.5 g porcine trypsin and 0.2 g EDTA • 4Na per liter of Hanks′Balanced Salt Solution with phenol red) were purchased from Merck. Calcium chloride dehydrate 99% and ethanol absolute ⩾99.8% AnalaR NORMAPUR® were purchased from VWR International. Low melting point alloy (LMPA) (Rose's A alloy, composed by Bi 54%, Pb 28%, Sn 18%) was obtained as a free sample from 5 N Plus, Germany. 9008 series borosilicate glass particles (8 μm diameter), calcein-AM and propidium iodide (Invitrogen™) were purchased from Thermo Fisher Scientific. AFM all-in-one-Al tips were purchased from budget sensors.

4.2. Microfluidic device fabrication

The microfluidic device was made of polydimethylsiloxane (PDMS) using standard soft photolithography techniques [52, 53]. PDMS (Sylgard 184, Dow, base elastomer: curing agent = 10:1) was degassed, casted, and baked at 70 °C for 1.5 h. The PDMS device was then sealed onto a standard microscope glass slide of 1 mm thickness via corona discharge treatment. To enable the application a temperature gradient, we employ a modified version of a microfluidic platform introduced earlier [24, 54, 55]. Briefly, the microfluidic device consisted of a straight main channel for hydrogel fabrication flanked by two parallel side channels (figures 1(b) and (c)). To provide a heating source, one side channel was filled with LMPA and then connected to a power supply unit, which acts as a Joule heater. On the other hand, room temperature water was continuously flowed through the other side channel using a syringe pump to act as a heat

sink, thus creating a temperature difference across the width of the main channel. A small reservoir was also cut out at one end of the main channel to allow extrusion of the substrate post-fabrication. The main channel is separated from the side channels by a 200 μm-thick PDMS wall. The height of all the microfluidic channels was 140 μm, with the channel length being 4 cm.

4.3. GG hydrogel fabrication

0.8%, 1% or 1.5% w/v of GG powder was dispersed in deionized water at 70 °C while stirring it until completely dissolved, then 5 mM of $CaCl_2$ was added as crosslinker. The hot GG/$CaCl_2$ solution was quickly injected into the main microfluidic channel until it overfilled at both ends, whereby the excess solution would crosslink rapidly upon exposure to ambient conditions, forming hydrogel plugs to close the channel. Meanwhile, the rest of the microfluidic chip was kept warm at 72 °C by placing it on a thermoelectric Peltier module (40 mm × 40 mm, RS components), which maintained the polymer solution in its uncrosslinked state.

A temperature gradient ranging from 3.6 to 7.5 °C mm^{-1} was applied across the sample channel for 20–30 min by setting the water flowrate constant at 300 μl min^{-1} using a syringe pump, and varying the power supply unit settings. After the concentration gradient was formed, the temperature gradient was removed and by switching the Peltier module to cooling mode, we were able to decrease the device temperature down to 0.5 °C within 1–2 min. This enabled rapid crosslinking and prevented disruption to the concentration gradient.

After 20 min, the GG gradient hydrogel was extruded from the microfluidic channel, attached to a poly (ethyleneimine)-coated glass slide, and stored in deionized water at 4 °C to prevent dehydration. To functionalize the glass slide, standard microscopy glass slides were first pretreated by corona discharge and then immersed in an aqueous solution containing 0.1% w/v poly (ethyleneimine) for at least 20 min. Finally, the glass slides were rinsed with deionized water and air-dried before use. This functionalization step induces a positive charge on the surface of glass slide, and thus, promotes adhesion of negatively charged GG hydrogels for AFM characterization and cell culture.

4.4. Temperature evaluation

While a temperature gradient was applied, temperatures of the 'hot' and 'cold' channels were measured using thermocouples inserted into each of the side channels. Subsequently, the actual temperature gradient across the sample microchannel can be estimated from these measurements and known thermal conductivities of the materials of the microfluidic device, assuming a linear gradient profile and using an electrical resistance analogy model (figure S2) [24].

4.5. AFM measurements

Young's moduli of the fabricated gels were characterized via indentation measurements using an atomic force microscope (JPK Nanowizard II). A micromanipulation technique [56] was used to attach a 8 μm diameter borosilicate glass sphere to an aluminum coated tipless cantilever. Substrates were immersed in deionized water to prevent dehydration, and then a 50 nN force was applied to the substrate surface. The force-displacement approach curve was fitted with the Hertz model for parabolical surfaces, with a Poisson ratio of 0.5, in order to obtain the Young's modulus value for each curve. Measurements were conducted at four equally spaced locations across the width of the substrate, taking care to avoid the edges to prevent any misrepresentation of the stiffness due to the friction experienced during extrusion from the microchannel. We obtained a local value of Young's modulus at each location by averaging 15 individual measurements obtained over a 20 μm × 20 μm area. Each stiffness gradient plot represents data obtained from a single substrate. For the initial test as reported in figure 1(d), stiffness measurements were also taken at 3–4 different locations along the length of sample to verify that the stiffness gradient was uniform along the sample.

4.6. SEM imaging

SEM was used to examine the native pore size across the hydrogel surface. To prepare samples for SEM imaging, the fabricated hydrogels were first subject to a solvent exchange process over 24 h to slowly replace water with ethanol. Briefly, in a petri dish, 0.3 ml deionized water was pipetted on the sample and then by using a syringe pump 20 ml of ethanol were dispensed over 24 h to the container. Subsequently, samples were transferred to microporous specimen capsules (78 μm pore size, Agar Scientific) and dried by supercritical CO_2 (Quorum E3100 critical point dryer, 4–5 flushes with liquid CO_2 and 15 min incubation between each flush) [57]. The samples were sputter-coated with 15 nm iridium (Qurum K575X) and then imaged using FEI Verios 460 SEM at 2 KeV and 25–50 pA probe current. The extracted SEM images were processed with ImageJ software to obtain the pore size distribution of each section (see supplementary material and supplementary figure S1).

4.7. Cell culture

All cell culture experiments were performed using GG gradient hydrogels prepared using 1% w/v initial GG concentration, with a temperature gradient of 7.5 °C mm^{-1} and 30 min application time. GG substrates mounted to PEI-coated glass slides were sterilized under UV lamp (11 W, 254 nm) for 10 min and transferred to a 6-well plate before use. MC3T3 osteoprogenitor cells were seeded on top of the substrate at a seeding density of 5000 cells mm^{-2} (for live/dead assay) or 20 000 cells mm^{-2} (for XRF study), followed

by incubation at 37 °C at 5% CO_2 for 3 h to allow cell attachment. Then, each well was filled with 3 mL of α-MEM cell culture medium, refreshed every 3 d and kept in the incubator. As a control experiment, MC3T3 cells were cultured onto GG hydrogels of a uniform Young's modulus, prepared using 1% w/v GG concentration.

4.8. Cell viability, attachment, proliferation, and migration studies

Live/dead assays were carried out to assess cells survival, adhesion, and proliferation by staining the cells with calcein-AM (Invitrogen™) and propidium iodide (Invitrogen™) at a concentration of 2.5 μl ml^{-1} and 5 μl ml^{-1}, respectively. Fluorescent images were captured at days 1, 3 and 7 of incubation using a confocal laser scanning microscope (OLYMPUS FV1000 Fluoview) coupled to a 10x fluorescent objective. In addition, cells were also labeled with PKH67 green fluorescent cell linker (Sigma Aldrich), a cell membrane dye, which enabled observation of cell migration across the substrates over 7 d. The cell viability experiments were performed in triplicate. Cell morphological assessments were performed on three uniform stiffness samples and one stiffness gradient sample. To compare the cell behavior between the softer and stiffer regions of the gradient sample, confocal image of the full length of hydrogel (obtained by stitching multiple images that were acquired side-by-side) was first segmented along the width axis into three strips, each 200 μm thick as shown in figure 4(b) (right). Note that the middle segment was excluded from subsequent analysis, to allow a clearer distinction between 'low' and 'high' substrate stiffness and their impact on cell behavior. Cell spreading was evaluated using $n = 39$ and $n = 99$ cells that were successfully segmented from the soft and stiff regions on the substrate, respectively. Additionally, cell density was evaluated by counting the number of cells in three randomly sampled areas for each analyzed condition.

4.9. XRF imaging

XRF analysis was performed to detect calcium and phosphate deposition. Osteoprogenitor cells were seeded on the surface of the substrates and cultured for up to 30 d, using normal (α-MEM) or osteogenic (α-MEM supplemented with ascorbic acid and glycerol-2-phosphate) media. At day 15 or 30, samples were washed with PBS and deionized water, then dried at room temperature for 20 min. Later, they were placed on the Bruker M4 Tornado XRF for x-ray imaging which was conducted at 50 keV under vacuum. All experiments were performed in triplicate.

4.10. Computational simulation

3D steady state numerical simulations were performed in ANSYS Fluent 2022 on a finite element mesh built around the same vector file used in the photolithography masking process. To model heat transfer through the polymer and the glass slide, we expanded the default Fluent materials library to include the thermal properties of PDMS and solid glass. Convective cooling was applied to all faces except the base of the glass plate, which contacted the Peltier. The Peltier and LMPA were modeled as interfaces of constant temperature, using values that had previously been experimentally measured [24]. The <1.5% w/v GG sample was treated as having the thermal properties of liquid water. We simulated the experimental conditions for 3.6 °C mm^{-1}, 4.5 °C mm^{-1}, and 5.4 °C mm^{-1} applied temperature gradients. The temperature gradient profile across the width of the sample was evaluated by inspecting the temperatures at the middle cross-sectional plane of the simulated microfluidic device. Temperature distributions along the length of the sample channel were extracted by taking vertex averages at 100 equidistant points.

Data availability statements

All data that support the findings of this study are included within the article (and any supplementary files).

Acknowledgments

We thank Professor Zhibing Zhang who granted us access to the Micromanipulation rig of his group. Also, we would like to acknowledge Dr Leslie Labarre and Dr Javier Marques de Marino for the training of AKP on both the micromanipulator and the AFM, Dr Erik Hughes for the XRF training and Dr Owen Davies and Dr Sophie C. Cox and her research group for the biological training and the consulting in the experimental section.

Funding sources

D V acknowledges the support from the EPSRC First Grant (EP/R004382/1). T P J K thank the Wellcome Trust and BBSRC for financial support.

Author contributions

Alexandros Kosmidis Papadimitriou: Investigation, Methodology, Writing—original draft. **Shin Wei Chong**: Investigation, Validation, Writing—review & editing. **Yi Shen**: Investigation, Writing—review & editing. **Oisin Stefan Lee**: Investigation, Validation. **Tuomas P J Knowles**: Resources, Supervision, Writing—review & editing. **Liam M Grover**: Resources, Supervision, Writing—review & editing. **Daniele Vigolo**: Conceptualization, Funding acquisition, Supervision, Writing—review & editing.

Conflict of interest

The authors declare no competing interests.

ORCID iDs

Alexandros Kosmidis Papadimitriou https://orcid.org/0000-0002-1654-4630
Shin Wei Chong https://orcid.org/0009-0004-7206-828X
Yi Shen https://orcid.org/0000-0002-0456-3850
Oisin Stefan Lee https://orcid.org/0009-0002-0611-0342
Daniele Vigolo https://orcid.org/0000-0002-8265-9882

References

[1] Madl C M and Heilshorn S C 2018 Engineering hydrogel microenvironments to recapitulate the stem cell niche *Annu. Rev. Biomed. Eng.* **20** 21–47
[2] Lutolf M P, Gilbert P M and Blau H M 2009 Designing materials to direct stem-cell fate *Nature* **462** 433–41
[3] Rozario T and DeSimone D W 2010 The extracellular matrix in development and morphogenesis: a dynamic view *Dev. Biol.* **341** 126–40
[4] Hayward M-K, Muncie J M and Weaver V M 2021 Tissue mechanics in stem cell fate, development, and cancer *Dev. Cell* **56** 1833–47
[5] Pelham R J and Wang Y L 1997 Cell locomotion and focal adhesions are regulated by substrate flexibility *Proc. Natl Acad. Sci. USA* **94** 13661–5
[6] Kuo C H R, Xian J, Brenton J D, Franze K and Sivaniah E 2012 Complex stiffness gradient substrates for studying mechanotactic cell migration *Adv. Mater.* **24** 6059–64
[7] Schrader J, Gordon-Walker T T, Aucott R L, van Deemter M, Quaas A, Walsh S, Benten D, Forbes S J, Wells R G and Iredale J P 2011 Matrix stiffness modulates proliferation, chemotherapeutic response, and dormancy in hepatocellular carcinoma cells *Hepatology* **53** 1192–205
[8] Engler A J, Sen S, Sweeney H L and Discher D E 2006 Matrix elasticity directs stem cell lineage specification *Cell* **126** 677–89
[9] Hadden W J *et al* 2017 Stem cell migration and mechanotransduction on linear stiffness gradient hydrogels *Proc. Natl Acad. Sci. USA* **114** 5647–52
[10] Sunyer R *et al* 2016 Collective cell durotaxis emerges from long-range intercellular force transmission *Science* **353** 1157–61
[11] Levental K R *et al* 2009 Matrix crosslinking forces tumor progression by enhancing integrin signaling *Cell* **139** 891–906
[12] Genin G M, Kent A, Birman V, Wopenka B, Pasteris J D, Marquez P J and Thomopoulos S 2009 Functional grading of mineral and collagen in the attachment of tendon to bone *Biophys. J.* **97** 976–85
[13] Thomopoulos S, Williams G R, Gimbel J A, Favata M and Soslowsky L J 2003 Variation of biomechanical, structural, and compositional properties along the tendon to bone insertion site *J. Orthop. Res.* **21** 413–9
[14] Marklein R A and Burdick J A 2009 Spatially controlled hydrogel mechanics to modulate stem cell interactions *Soft Matter* **6** 136–43
[15] Sunyer R, Jin A J, Nossal R, Sackett D L and Leipzig N D 2012 Fabrication of hydrogels with steep stiffness gradients for studying cell mechanical response *PLoS One* **7** e46107
[16] Zaari N, Rajagopalan P, Kim S K, Engler A J and Wong J Y 2004 Photopolymerization in microfluidic gradient generators: microscale control of substrate compliance to manipulate cell response *Adv. Mater.* **16** 2133–7
[17] Xin S, Dai J, Gregory C A, Han A and Alge D L 2020 Creating physicochemical gradients in modular microporous annealed particle hydrogels via a microfluidic method *Adv. Funct. Mater.* **30** 1907102
[18] Hopp I, Michelmore A, Smith L E, Robinson D E, Bachhuka A, Mierczynska A and Vasilev K 2013 The influence of substrate stiffness gradients on primary human dermal fibroblasts *Biomaterials* **34** 5070–7
[19] Vincent L G, Choi Y S, Alonso-latorre B, Del Álamo J C and Engler A J 2013 Mesenchymal stem cell durotaxis depends on substrate stiffness gradient strength *Biotechnol. J.* **8** 472–84
[20] Tse J R and Engler A J 2010 Preparation of hydrogel substrates with tunable mechanical properties *Curr. Protoc. Cell Biol.* **47** 10.16.1–10.16.16
[21] Blache U, Ford E M, Ha B, Rijns L, Chaudhuri O, Dankers P Y W, Kloxin A M, Snedeker J G and Gentleman E 2022 Engineered hydrogels for mechanobiology *Nat. Rev. Method Primers* **2** 98
[22] Oh S H, An D B, Kim T H and Lee J H 2016 Wide-range stiffness gradient PVA/HA hydrogel to investigate stem cell differentiation behavior *Acta Biomater.* **35** 23–31
[23] Wang P-Y, Tsai W-B and Voelcker N H 2012 Screening of rat mesenchymal stem cell behaviour on polydimethylsiloxane stiffness gradients *Acta Biomater.* **8** 519–30
[24] Vigolo D, Ramakrishna S N and DeMello A J 2019 Facile tuning of the mechanical properties of a biocompatible soft material *Sci. Rep.* **9** 7125
[25] Vigolo D, Rusconi R, Stone H A and Piazza R 2010 Thermophoresis: microfluidics characterization and separation *Soft Matter* **6** 3489–93
[26] Caliari S R and Harley B A C 2014 Structural and biochemical modification of a collagen scaffold to selectively enhance MSC tenogenic, chondrogenic, and osteogenic differentiation *Adv. Healthcare Mater.* **3** 1086–96
[27] Miyoshi E, Takaya T and Nishinari K 1996 Rheological and thermal studies of gel-sol transition in gellan gum aqueous solutions *Carbohydrate Polym.* **30** 109–19
[28] Tang J, Tung M A and Zeng Y 1997 Gelling properties of gellan solutions containing monovalent and divalent cations *J. Food Sci.* **62** 688–712
[29] Coutinho D F, Sant S V, Shin H, Oliveira J T, Gomes M E, Neves N M, Khademhosseini A and Reis R L 2010 Modified Gellan Gum hydrogels with tunable physical and mechanical properties *Biomaterials* **31** 7494–502
[30] Stevens L R, Gilmore K J, Wallace G G and In het Panhuis M 2016 Tissue engineering with gellan gum *Biomater. Sci.* **4** 1276–90
[31] Vieira S, da Silva Morais A, Garet E, Silva-Correia J, Reis R L, González-Fernández Á and Miguel Oliveira J 2019 Self-mineralizing Ca-enriched methacrylated gellan gum beads for bone tissue engineering *Acta Biomater.* **93** 74–85
[32] Piazza R 2008 Thermophoresis: moving particles with thermal gradients *Soft Matter* **4** 1740–4
[33] Piazza R and Parola A 2008 Thermophoresis in colloidal suspensions *J. Phys.: Condens. Matter* **20** 153102
[34] Braibanti M, Vigolo D and Piazza R 2008 Does thermophoretic mobility depend on particle size? *Phys. Rev. Lett.* **100** 108303
[35] Vigolo D, Brambilla G and Piazza R 2007 Thermophoresis of microemulsion droplets: size dependence of the Soret effect *Phys. Rev.* E **75** 040401
[36] Iacopini S, Rusconi R and Piazza R 2006 The "macromolecular tourist": universal temperature dependence of thermal diffusion in aqueous colloidal suspensions *Eur. Phys. J.* E **19** 59–67
[37] Vigolo D, Buzzaccaro S and Piazza R 2010 Thermophoresis and thermoelectricity in surfactant solutions *Langmuir* **26** 7792–801
[38] Tang J, Tung M A and Zeng Y 1997 Gelling temperature of gellan solutions containing calcium ions *J. Food Sci.* **62** 276–80

[39] Coviello T, Matricardi P, Marianecci C and Alhaique F 2007 Polysaccharide hydrogels for modified release formulations *J. Control. Release* **119** 5–24
[40] Kirch J, Schneider A, Abou B, Hopf A, Schaefer U F, Schneider M, Schall C, Wagner C and Lehr C-M 2012 Optical tweezers reveal relationship between microstructure and nanoparticle penetration of pulmonary mucus *Proc. Natl Acad. Sci. USA* **109** 18355–60
[41] Wen J H, Vincent L G, Fuhrmann A, Choi Y S, Hribar K C, Taylor-Weiner H, Chen S and Engler A J 2014 Interplay of matrix stiffness and protein tethering in stem cell differentiation *Nat. Mater.* **13** 979–87
[42] Rehfeldt F, Engler A J, Eckhardt A, Ahmed F and Discher D E 2007 Cell responses to the mechanochemical microenvironment-implications for regenerative medicine and drug delivery *Adv. Drug Deliv. Rev.* **59** 1329–39
[43] Huebsch N, Arany P R, Mao A S, Shvartsman D, Ali O A, Bencherif S A, Rivera-Feliciano J and Mooney D J 2010 Harnessing traction-mediated manipulation of the cell/matrix interface to control stem-cell fate *Nat. Mater.* **9** 518–26
[44] Hou Y, Yu L, Xie W, Camacho L C, Zhang M, Chu Z, Wei Q and Haag R 2020 Surface roughness and substrate stiffness synergize to drive cellular mechanoresponse *Nano Lett.* **20** 748–57
[45] Engler A, Bacakova L, Newman C, Hategan A, Griffin M and Discher D 2004 Substrate compliance versus ligand density in cell on gel responses *Biophys. J.* **86** 617–28
[46] Doss B L, Pan M, Gupta M, Grenci G, Mège R-M, Lim C T, Sheetz M P, Voituriez R and Ladoux B 2020 Cell response to substrate rigidity is regulated by active and passive cytoskeletal stress *Proc. Natl Acad. Sci. USA* **117** 12817–25
[47] Isenberg B C, DiMilla P A, Walker M, Kim S and Wong J Y 2009 Vascular smooth muscle cell durotaxis depends on substrate stiffness gradient strength *Biophys. J.* **97** 1313–22
[48] Khatiwala C B, Peyton S R and Putnam A J 2006 Intrinsic mechanical properties of the extracellular matrix affect the behavior of pre-osteoblastic MC3T3-E1 cells *Am. J. Physiol. Cell Physiol.* **290** 1640–50
[49] Zhang T, Lin S, Shao X, Zhang Q, Xue C, Zhang S, Lin Y, Zhu B and Cai X 2017 Effect of matrix stiffness on osteoblast functionalization *Cell Prolif.* **50** e12338
[50] Sun M, Chi G, Xu J, Tan Y, Xu J, Lv S, Xu Z, Xia Y, Li L and Li Y 2018 Extracellular matrix stiffness controls osteogenic differentiation of mesenchymal stem cells mediated by integrin α5 *Stem Cell Res. Ther.* **9** 52
[51] Ko H *et al* 2019 A simple layer-stacking technique to generate biomolecular and mechanical gradients in photocrosslinkable hydrogels *Biofabrication* **11** 025014
[52] Xia Y and Whitesides G M 1998 Soft lithography *Annu. Rev. Mater. Sci.* **28** 153–84
[53] Mcdonald J C, Duffy D C, Anderson J R, Chiu D T, Wu H, Schueller O J and Whitesides G M 2000 Fabrication of microfluidic systems in poly(dimethylsiloxane) *Electrophoresis* **21** 27–40
[54] Vigolo D, Zhao J, Handschin S, Cao X, DeMello A J and Mezzenga R 2017 Continuous isotropic-nematic transition in amyloid fibril suspensions driven by thermophoresis *Sci. Rep.* **7** 1211
[55] Vigolo D, Rusconi R, Piazzaa R and Stone H A 2010 A portable device for temperature control along microchannels *Lab Chip* **10** 795–8
[56] Zhang Z, Ferenczi M A and Thomas C R 1992 A micromanipulation technique with a theoretical cell model for determining mechanical properties of single mammalian cells *Chem. Eng. Sci.* **47** 1347–54
[57] Shen Y, Nyström G and Mezzenga R 2017 Amyloid fibrils form hybrid colloidal gels and aerogels with dispersed $CaCO_3$ nanoparticles *Adv. Funct. Mater.* **27** 1700897